EFFECT OF LOW AND EXTREME-LOW TEMPERATURE ON MECHANICAL PROPERTIES OF 3D-PRINTED POLYETHYLENE TEREPHTHALATE GLYCOL

FELICIA STAN[1], NICOLETA-VIOLETA STANCIU[1], IONUŢ-LAURENŢIU SANDU[1], CĂTĂLIN FETECĂU[1*], ALEXANDRU ŞERBAN[2]

Abstract. This paper investigates the mechanical behavior of 3D-printed Polyethylene Terephthalate Glycol (PETG) before and after exposure to low and extreme-low temperature. Before printing, melt shear viscosity of the PETG was investigated as a function of temperature and shear rate to evaluate its flowability. 3D-printed PETG specimens with four different patterns (full, circular, honeycomb, and strip) were subjected to deep cryogenic treatment for 24 h, and thermal annealing cycles at –40°C. Tension tests were performed to evaluate the mechanical properties of the 3D-printed samples before and after thermal treatments. Experimental results show that mechanical properties of the 3D-printed samples have a close relationship with the printing pattern. The honeycomb specimens exhibit the highest specific strength (tensile strength/ weight) among the other 3D printing patterns. No statistical significant alterations of mechanical properties are observed after exposure to thermal annealing cycles at –40°C, indicating that this material may be successfully used to manufacture parts that will be exposed to low temperatures during operation. The mechanical properties of the cryogenically treated samples decrease significantly as compared with the un-treated samples for the same printing conditions. However, depending on the printing pattern, the 3D-printed PETG samples maintain at least 75% of its untreated mechanical properties after the cryogenic treatment.

Key words: cryogenic, mechanical properties, additive manufacturing, Polyethylene Terephthalate Glycol copolymer.

1. INTRODUCTION

In the last years, due to the ability to fabricate complex, lightweight objects with unique properties and functionality [1–5], the 3D printing technologies have been playing a key role in several industries such as automotive, aerospace and

[1] Center of Excellence Polymer Processing, "Dunarea de Jos" University of Galati, 47 Domneasca, 800008, Galati, Romania
[2] "Politehnica" University of Bucharest, 313 Splaiul Independentei, Bucharest, Romania
*Corresponding author: Cătălin Fetecău, catalin.fetecau@ugal.ro

Ro. J. Techn. Sci. – Appl. Mechanics, Vol. 64, N° 1, P. 21–41, Bucharest, 2019

defense, and others including healthcare. For instance, in 2016, revenues from automotive applications amounted to over $3.9 billion, and about $2.4 billion from aerospace and defense applications [6,7], while the additive manufacturing industry grew 25.9% corporate annual growth rate (CAGR) to $5.165 billion in 2015 [7]. According to the latest market analysis reports, the demand on 3D-printing is on significant rise. The global spending on 3D-printing, which includes hardware, materials, software, and related services, is expected to exceed $14.0 billion in 2019, an increase of 23.2% over 2018, and reach $23.0 billion in 2022 with a five-year CAGR of 18.4% [8]. Moreover, considerably high revenues from medical and dental applications are also expected in the next years. For dental and medical support objects, including tissue, organ and bone printing, a five-year CAGR exceeding 21% is predicted in 2019 [8].

The 3D-printing technologies are primarily used in prototyping, product development, and innovation in the automotive industry, aerospace industry, medical industry etc. [9, 10]. However, in the last years, the 3D-printing technology has also been applied to create real-life applications, from athletic shoes to vehicle interiors, and from apparel to personalized medical devices. The 3D-printing technology is also a desirable option when one need to replace parts (spare parts) from discontinued equipments or devices since the old technical drawing is simply converted into a CAD file and printed, resulting a part that is cheaper, stronger and lighter that the original one. With home 3D printers available at reasonable prices, another trend that becomes more and more striking over the years is the use of 3D-printing in schools, public libraries and homes that will have a large impact on creativity and innovation [11, 12].

Regardless of the applications, a good design of a 3D-printed part is to have excellent quality with minimal anisotropy [1–5]. However, mechanical properties, including mechanical anisotropy (part-to-part and intra-part variations) pose the largest problem in manufacturing with 3D-printing [13–16]. The mechanical properties of 3D-printed parts (stiffness, tensile strength, stress and strain at break) can be affected by a number of factors, including the filament properties (density, molecular weight, type and quality, etc.), the AM process parameters (bed and extrusion temperatures, printing orientation, layer size, infill pattern and%, cross-section area), and post-processing (method and time) [17–23]. Residual stresses, which are developed due to the thermal expansion or contraction during 3D-printing, also influence the strength of 3D-printed parts [24–27]. Thus, it is very difficult to control the mechanical properties of the 3D-printed part and predict how it would behave given a certain mechanical load.

The question as to what material property should be considered for designing a 3D-printing part now arises. In general, in the absence of standards for 3D-printing, it is recommended to design the 3D-printed part such that the load in the part is aligned with the strongest orientation of the printed material [4, 28]. However, for practical applications, the weakest property of the 3D-printed part may be considered

for design factor (what the part is required to be able to withstand), but it would be best if the relationships of processing parameters and mechanical properties can be fully understood [17, 18, 29, 30].

Due to distinct advantages over conventional fabrication techniques, 3D-printing technologies promise solutions for aerospace field for which components with a combination of lightweight and high mechanical properties for extreme loading conditions are continuously sought [31].

Understanding the mechanical behavior of 3D-printed parts from very low to very high temperatures is particularly important for space applications, since they must function through a broad operating temperature range, from very low to high temperatures. For example, the temperature in the International Space Station ranges from −157°C to 121°C [32]. On the other hand, due to possible evolution of the micro-structure during the exposure of plastics to low or high temperatures (e.g. plastics will generally become stronger, stiffer and more brittle in cryogenic temperature [33], and display reduced strength and elongation after long term exposure to elevated temperature) it is important to know not only the required strengths for each application, but also the mechanical properties of the 3D-printed parts after long-term exposure to various environmental conditions (e.g. residual mechanical properties). Most of the research papers focus on mechanical properties of 3D-printed components at room temperature and how they are affected by various process parameters [17–19, 34–37]. Only few papers reports on mechanical properties at cryogenic temperatures [38–40] or realistic environmental conditions [41]. Preservation of mechanical properties of 3D-printed structures after exposure to extreme environmental conditions plays an important role in the design to manufacturing parts by 3D-printing for space applications; unfortunately, no studies are available on the mechanical behavior of 3D-printed structures after exposure to low and extremely low temperature (cryogenic temperature).

Thus, this research is focused on mechanical properties of 3D-printed PETG parts after exposure to low, –40°C, and extreme low, –196°C, temperatures. Before printing, the PETG filament was characterized in terms of melt shear viscosity, to evaluate its flow features during printing, and mechanical properties. To study the effect of cryogenic treatment on the mechanical behavior of the PETG, 3D-printed specimens were subjected to deep cryogenic temperature by quench method. In addition, 3D-printed specimens were subjected to low temperature thermal annealing cycles at –40°C. The influence to residual mechanical properties is discussed.

2. MATERIALS AND METHODS

2.1. Material for 3D printing

The material considered in this research is a glycol modified version of Polyethylene Terephthalate (3DXNano™ ESD-Safe PETG, 3DXTECH, USA) with a surface resistance of 10^7 to 10^9 Ohm [42].

PETG is designed for use in 3D-printing applications that require electrostatic discharge protection and a high level of cleanliness. For this material, the recommended printing temperature is 230 to 260°C [42].

2.2. Filament characterization

Melt flow index. To study the influence of temperature on the PETG flow behavior, the melt flow index (MFI) of PETG was measured using the Melt Flow Index Tester (CEAST Model 7021-7022, Instron, USA) with an applied load of 2.16 kg (MFI_2) at 235, 245 and 255°C, respectively, and the results were expressed in grams per 10 min (three times per sample). In addition, the MFI was measured with a mass of 5 kg (MFI_5) at 255°C, and the MFI_5/MFI_2 ratio was referred to as the melt flow rate (MFR).

Melt shear viscosity. Melt viscosity is a key parameter to consider when setting process parameters for 3D-printing. Therefore, the viscosity of the PETG was measured under a temperature range of 235 to 255°C, to evaluate its flow features during printing. A high pressure capillary rheometer (Rheograph RG75, Göttfert, Germany) was used for the measurement of melt shear viscosities at low to medium shear rates (50 to 2000 s^{-1}). This rheometer was equipped with three round capillaries with 1 mm diameter and length of 10, 20 and 30 mm, respectively. The PETG filament was cut into small pellets of 2 mm length and, before testing, the pellets were vacuum dried in oven at 80°C for 4 h.

Mechanical testing. PETG filament specimens of 100 mm length were directly cut from the PETG filament spool. A universal testing machine (Testometric AT 350, UK) with a 5000 N load cell was used to test the mechanical properties of the PETG filaments. Each filament specimen was fixed in the pneumatic griping system with a 50 mm gap. The test was carried out with a standard crosshead speed of 5 mm/min [43]. At least eight filament specimens were tested and analyzed.

2.3. 3D-printing of the PETG specimens

Specimens have been printed using the commercial 3D printer (X400 printer, 3D German RepRap) from a single spool of PETG filament with an initial diameter of 1.75 mm through a circular nozzle with diameter of 0.4 mm. The geometry of the specimens is presented in Fig. 1 (ISO 527 – type 1BA [43]). The 3D model of the specimens was modeled using Inventor software, exported as a stereolithography (STL) file, and sliced using the "Cura 15.02.1" software [44].

In order to investigate the effect of cross-section/pattern on the mechanical behavior of the 3D-printed specimens, in this research, four different patterns were considered [45], as shown in Fig. 2 (left to right): full, circular, honeycomb, and strip.

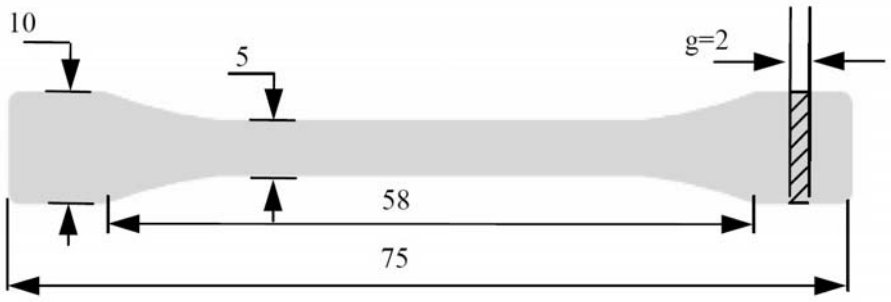

Fig. 1 – Geometry for tensile testing of 3D-printed parts (units in mm).

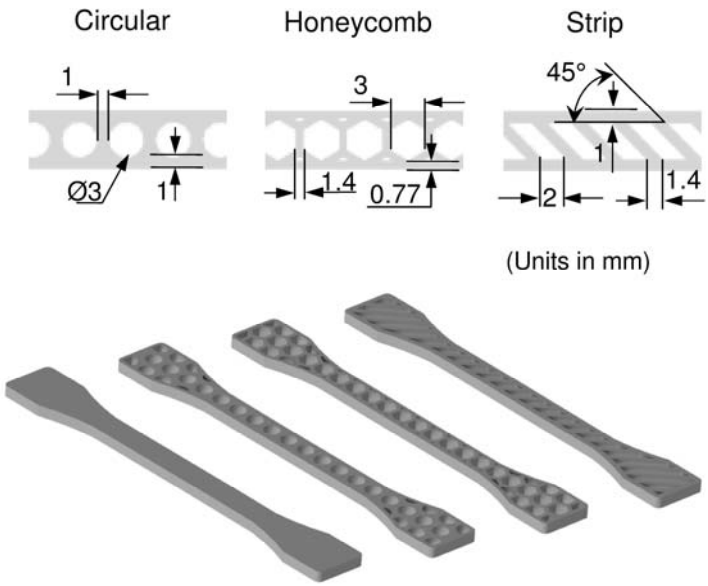

Fig. 2 – 3D view of specimens used for measurements of the mechanical response.

For the full cross-section, three printing directions (direction of material bead/road relative to the loading of the part) were considered 0, 45, and 90°, respectively, to investigate the influence of the layer orientation on the mechanical properties of the printed samples (Fig. 3). Prior to 3D-printing of specimens, a study on the sensitivity of the material to the printing parameters was conducted, especially the melt temperature and platform temperature. Several specimens were manufactured using different printing parameters and tested to measure their mechanical properties and to observe any features.

The ranges investigated were 240 to 260°C for the extrusion temperature, 60 to 80°C for the bed temperature, and 0.1 to 0.2 mm for the layer height. The optimal printing parameters were determined as 255°C for the extrusion temperature, 70°C

for the bed temperature, 0.14 mm for layer height, and 20 mm/s for the deposition speed. The fill percentage was set at 100% for all samples. Each sample was printed flat (lying in the *X*-*Y* plane, as shown in Fig. 3), individually, at the same position on the printing bed. All samples were printed using two wall-line counts with 0.4 mm wall thickness, 0.14 mm layer height (in the *Z* direction, Fig. 3), and 0 mm air gap. The height of the top and bottom layers was nearly equal for all specimens.

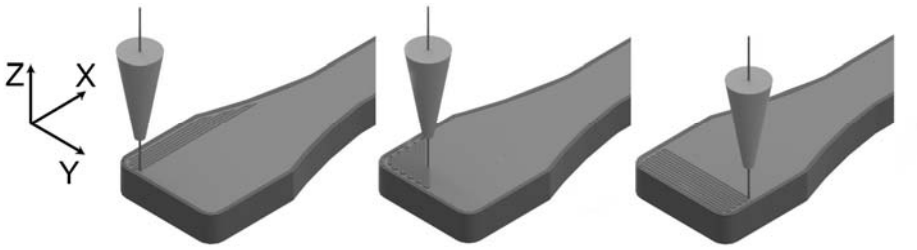

Fig. 3 – Printing direction relative to the loading of the specimen: 0°, 45° and 90° (left to right).

2.4. Characterization of 3D-printed specimens

Cryogenic treatment. To study the effect of cryogenic treatment on the mechanical behavior of the PETG, selected 3D-printed specimens were subjected to deep cryogenic temperature (DCT) by quench method (QM). The schematic diagram showing the configuration of the QM is presented in Fig. 4. In the QM, the 3D-printed samples were submerged in liquid nitrogen environment (LNT, −196°C) and maintained for 24h. In order to minimize the thermal shock and prevent micro-cracking from rapid cooling and direct contact with the liquid nitrogen, the 3D-printed samples were placed into an in-house design container, which in turn was placed into the cryo chamber. After the soaking period, the container was removed from the cryo chamber allowing the natural rate of worm-up to room temperature (RT, 23 ± 2°C).

Thermal annealing. Selected 3D-printed specimens were also subject to thermal annealing in a climatic test chamber (VC³7018, Vötsch Industrietechnik GmbH). This consisted of a gradual cooling from RT to a temperature of −40°C with a cooling rate of 1°C/min, a dwelling phase of 6 h and slow heating (1°C/min) to the room temperature. The annealing thermal cycle was repeated three 3 times, as shown in Fig. 4 (e.g. TA).

Mechanical tests. The untreated as well as the thermally treated specimens were tested in tension using the Testometric universal mechanical testing machine. All tests were performed at room temperature. Load and displacement were continuously measured throughout each test. The load was applied at a standard crosshead displacement of 5 mm/min [43]. At least five 3D-printed specimens were tested and analyzed.

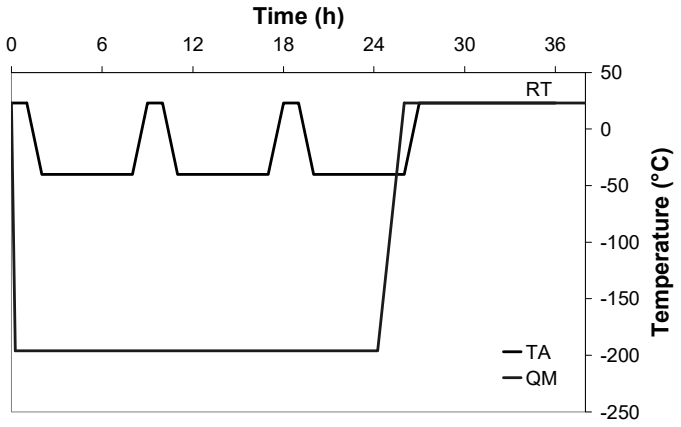

Fig. 4 – Schematic representation of the quench (QM) and thermal annealing (TA) methods.

The load-displacement curves were transferred into engineering stress-strain curves based on the nominal dimensions of the samples, including the CAD effective cross-section area.

Young modulus was calculated as the slope of the stress-strain relationship between 0.0025 and 0.005 strain, following ISO 527:2012 [43], while the tensile strength is given as the maximum tensile stress. The specific tensile strength was also calculated as the ratio between the tensile strength and the corresponding mass of specimen [45].

3. RESULTS AND DISCUSSION

3.1. Rheological properties of PETG filament

Table 1 summarizes the MFI for the PETG filament. The results show that the MFI increases with increasing melt temperature, indicating that the printing capability would improve with increasing melt temperature. As shown in Table 1, the value of the MFI_2 = 12.39g/10 min at 255°C is 4.6 times as the value of MFI_2 = 2.67 g/10 at 235°C. On the other hand, the PETG has a MFR (MFI_5/MFI_2 ratio) of 1.64 at 255°C, indicating its suitability for 3D printing.

Table 1

Melt flow index of PETG filament

Temperature [°C]	Mass [kg]	MFI [g/10 min]
235	2.16	2.67
245		3.77
255		12.39
255	5.0	20.35

Figure 5 shows the double log-log plot of apparent shear stress vs. apparent shear rate for different melt temperatures. It can be seen that the PETG behaves like a pseudo-plastic liquid, i.e., a straight line can be drawn over at least two to three decades of shear rate. Thus, the apparent shear stress as a function of apparent shear rate was described by a power law [46]

$$\tau = K\dot{\gamma}^n \tag{1}$$

where K is the consistency index (the larger the K the more viscous the melt), and n is the power law index ($n < 1$ for shear thinning). The power law parameters, calculated using the linear regression, are listed in Table 2.

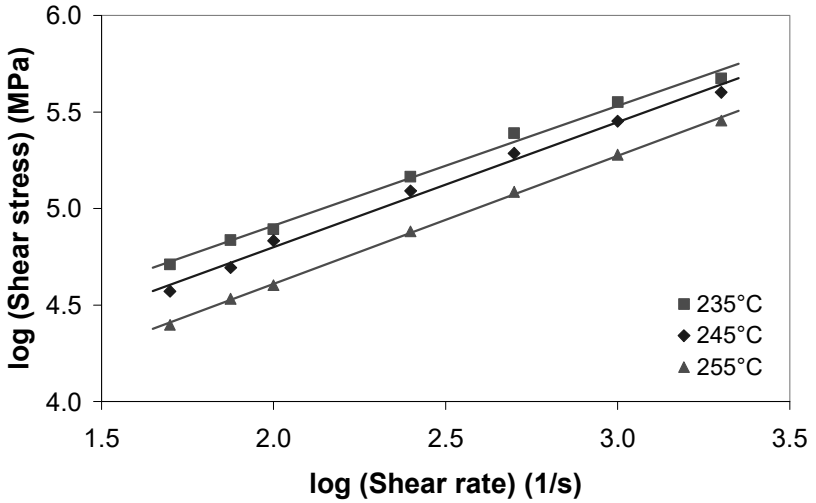

Fig. 5 – Apparent shear stress versus apparent shear rate (log-log) for PETG.

Table 2

Power law parameters

Temperature [°C]	K [Pa s^n]	n	R^2
235	4675.20	0.620	0.994
245	3207.01	0.647	0.993
255	1920.88	0.663	0.999

Figure 6 illustrates the melt shear viscosity as a function of reciprocal absolute temperature ($1/T$), for different shear rates. For every shear rate examined, the Arrhenius type dependence on temperature was observed, thus the activation energy for flow was determined from the slope (E_a/R, with E_a – activation energy and R – gas constant) of the Arrhenius plot (solid lines in Fig. 6). At low shear rates (1,000 s^{-1} and under), the PETG flow activation energy (80.42, 77.80, 69.97, and

72.26 k J/mol for 50, 75, 250 and 1,000 s^{-1}, respectively) decreases nonlinearly with increasing shear rate, suggesting a change of the flow mechanism as a result of structural modification of the PETG melt (change in the polymer structure).

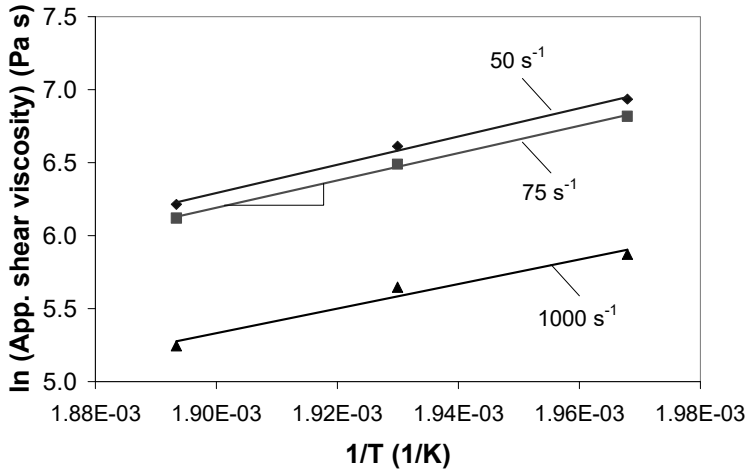

Fig. 6 – Temperature dependence of apparent melt shear viscosity.

Figure 7 presents the melt shear viscosity (Bagley and Rabinowitsch-Weissenberg corrections applied) as a function of shear rate during capillary extrusion of PETG for different melt temperatures, in a bi-logarithmic scale. In the investigated temperature range, the melt shear viscosity decreases linearly with increasing shear rate, indicating non-Newtonian flow behavior (shear thinning behavior, $n < 1$) nearly the entire range of the shear rate domain.

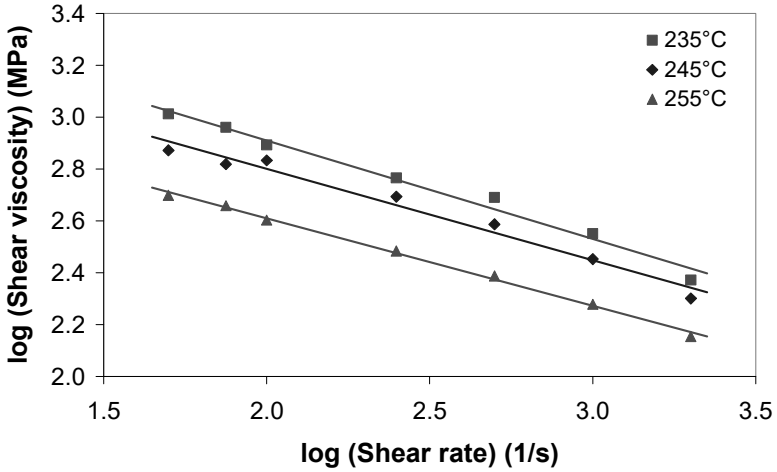

Fig. 7 – Melt shear viscosity of PETG at different melt temperatures.

3.2. Mechanical properties

Prior to tensile testing, all printed samples were individually inspected, weighted and measured to evaluate the printing accuracy (Table 3). The measured dimensions of the 3D-printed specimens were compared with nominal CAD dimensions. It is important to note that no major, visible defects were observed.

For the full cross-section, Table 3 shows a negligible effect of printing orientation on the specimen weight (less then 1% reduction in weight when the printing angle is changed from 0 to 45 and 90°). On the other hand, Table 3 indicates a substantial reduction in weight of approximately 50%, 35% and 35% for the honeycomb, circular and strip pattern specimens, respectively, as compared to 0° raster orientation (which is considered the base line).

The thickness of the 3D-printed samples is undersized except for circular pattern, which is oversized, as shown in Table 3. The undersizing of thickness is related to the thermal shrinkage of the roads during the printing process, and adhesion between the roads [47, 48]. As shown in Table 3, shrinkage tends to be smaller as the printing angle changes from 0°, to 45° and 90°. Taking the 45° and 90° for examples, due to the fact that the roads are shorter as compared with 0°, the contraction of the previously printed rods is restricted by the current road. The process continues as further layers are printed. However, the 3D-printed PETG samples shrink maximum 6%, although this varies depending on the printing pattern. The 45° samples have far less shrinkage (~2%).

Table 3

Dimensions of the 3D-printed samples

Property	Pattern/Cross-section					
	Strip	**Honeycomb**	**Circular**	**Full 0°**	**Full 45°**	**Full 90°**
Weight [g]	$0.760^{\pm 0.008}$	$0.582^{\pm 0.002}$	$0.760^{\pm 0.002}$	$1.176^{\pm 0.004}$	$1.172^{\pm 0.004}$	$1.167^{\pm 0.004}$
Thickness [mm]	$1.91^{\pm 0.043}$	$1.92^{\pm 0.074}$	$2.054^{\pm 0.024}$	$1.88^{\pm 0.033}$	$1.96^{\pm 0.019}$	$1.91^{\pm 0.034}$
Shrinkage [%]	4.35	4.17	–2.69	6.12	1.90	4.30

Figure 8 shows optical images of the 3D-printed specimens at three different printing orientations, both in-plane (*X*-*Y*) and out-of-plane (thickness, *X*-*Z*) directions. Figs. 8a and 8b show roads that were not well adhered to the adjacent roads in the in-plane, but well fused roads out-of-plane. Moreover, for the 45° raster orientation (Fig. 8b), between every other road there was a gap and the previously printed layer can be seen.

For the 90° orientation, Fig. 8c shows well fused roads both in the in-plane and out-of-plane directions. This is because for 90° orientation the printing path is shorter compared to 0° and 45° orientations and the polymer does not cool down before the next road is printed next to it. In summary, good quality printing process was produced with well fused out-of-plane roads and some inconsistently fused (non-contacting roads) in-plane roads.

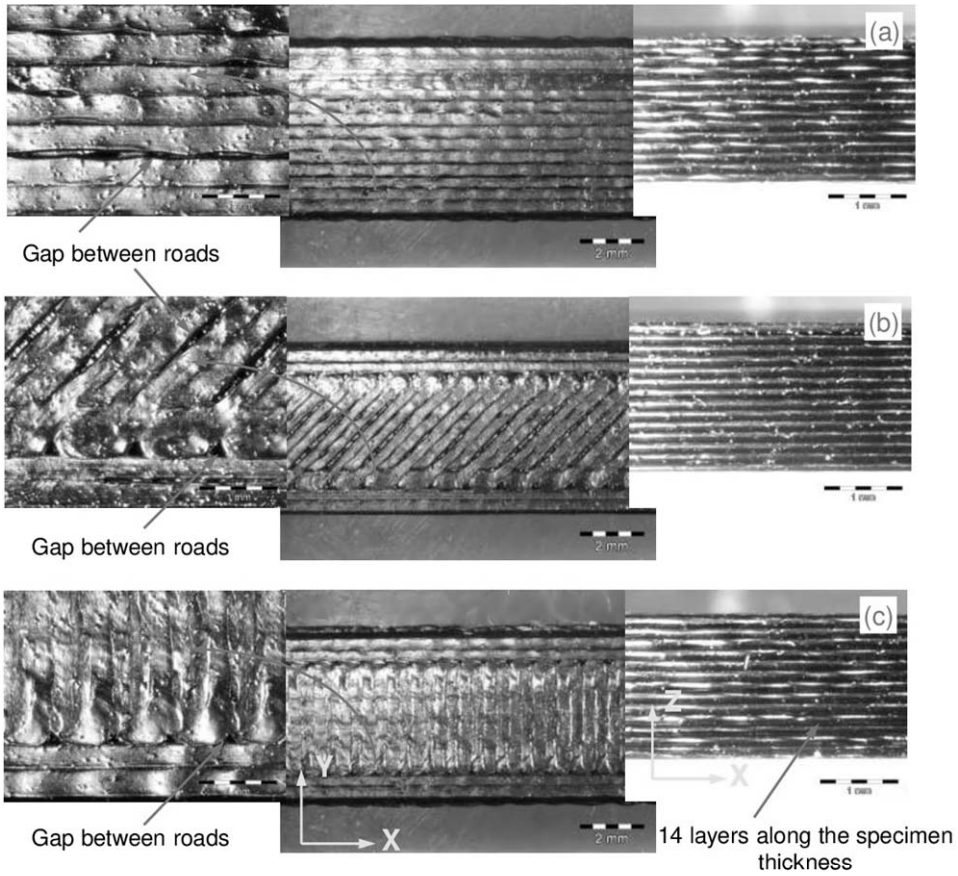

Fig. 8 – Optical micro-graphs (front *X*-*Y*, and thickness *X*-*Z* faces) of 3D-printed samples. Solid layers are oriented (a) 0°, (b) 45° and (c) 90° from the longitudinal axis.

Figure 9 shows the representative engineering stress-strain curve determined for the as-received PETG filament. PETG filament displays ductile elastic-plastic behaviour with a stiffness of 1626 ± 53.5 MPa and tensile strength of 43 ± 0.16 MPa.

To highlight the effect of printing direction on the mechanical properties, we compare, in Fig. 10, engineering stress-strain response under tension of the 3D-printed PETG for 0° and 90° printing directions. All 3D-printed samples

display a ductile behavior in tension, with small difference up to the maximum stress, between 0° printing direction (the blue curve), and 90° printing direction (the red curve). However, the tensile ductility of 90° specimens was 110% less in comparison to the 0° specimens.

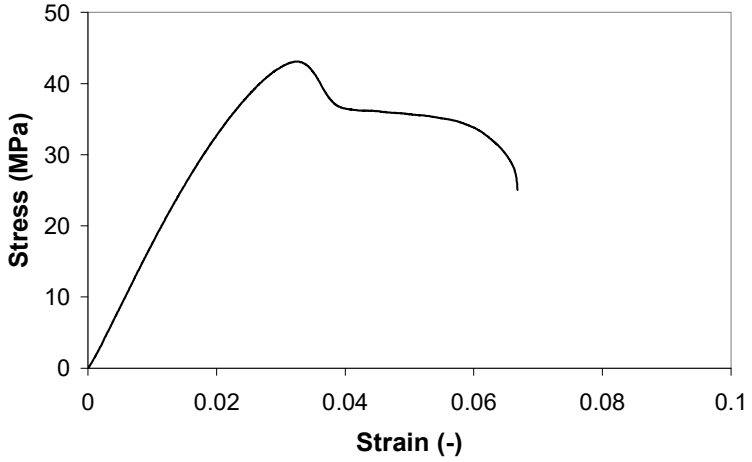

Fig. 9 – Engineering stress–strain curve for PETG filament at 5 mm/min.

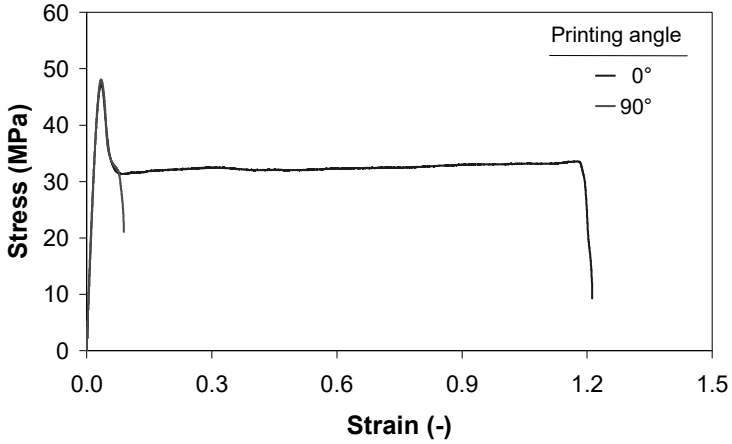

Fig. 10 – Engineering stress–strain curve for PETG filament at 5 mm/min.

Figure 11 shows the effect of the cross-section/pattern on the engineering stress–strain curves measured for the untreated 3D-printed samples. It can be seen that the 3D-printed samples with strip pattern (red curve) exhibit the highest tensile strength, while the specimens with circular pattern (green curve) display brittle behavior with substantial reduction in tensile strength and elongation at break (tensile ductility of only 2%).

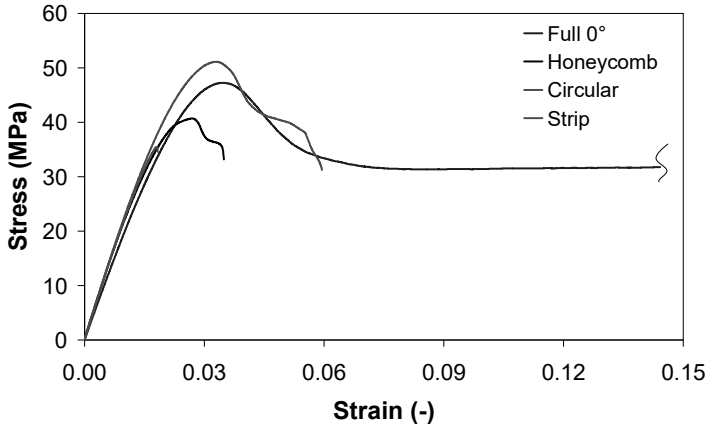

Fig. 11 – Effect of pattern on the engineering stress-strain curves of the untreated 3D-printed PETG samples.

The tensile response of circular, honeycomb, and strip pattern specimens was brittle, with average tensile ductility of order 2, 4 and 5%, respectively (Fig. 12). The 0° and 45° specimens, on the other hand, display a ductile elasto-plastic response with necking and tensile ductility of order 120% and 90%, respectively. Specimens with 90° printing orientation experienced a moderately ductile fracture (tensile ductility of order 10%) since failure occurs mainly in inter-raster fusion bonds [49], as shown in Fig. 12.

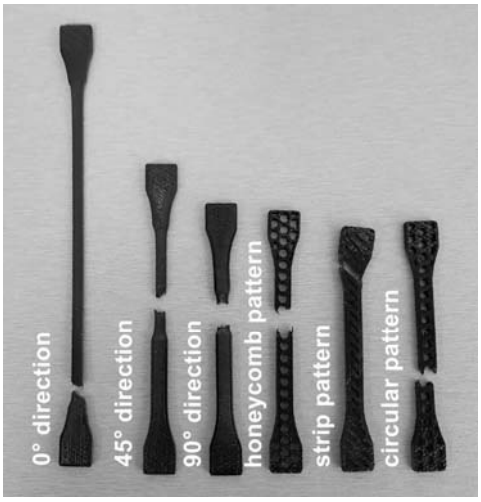

Fig. 12 – Fracture mode of 3D-printed PETG samples.

Compared to tensile strength of the PETG filament (Fig.9), the 3D-printed parts showed higher or comparable tensile strength except for the circular pattern, which exhibited much smaller tensile strength (about 20% lower). Taking 45° or 90°

printing orientation for examples, no significant difference in tensile strength between the PETG filament and 3D-printed samples is observed. This is most likely due to the high extruder temperature that created significant thermal bonding between roads and layers causing very good fusing [41].

Figure 13 shows the effect of thermal treatment on the mechanical properties of 3D-printed PETG specimens. The corresponding mechanical property values (the average and standard deviation of a set of five specimens) for each printed configuration are summarized in Tables 4 to 6.

It is important to note that while the stiffness and tensile strength were fairly similar between the specimens with the same batch (number of replicates), there was a large amount of variability in the strain at break, especially for the 45° pattern. However, the variation between specimens with the same batch was slightly higher for the cryogenically treated specimens than the untreated and thermally annealed specimens.

For the un-treated full cross-section parts (UT), when comparing the printing orientations, as shown in Fig. 13a and Table 4, it is observed that the Young modulus and the tensile strength for 0° orientation is only 2–3% higher than for 45° or 90° orientations, with no significant reduction in the weight. Furthermore, it is observed that the honeycomb pattern gives similar elastic modulus (2368.25 ± 23.65 MPa) to the circular and strip patterns (2353.50 ± 18.30 MPa and 2321.60 ± 27.76 MPa, respectively), but with approximately 25% weight reduction. The tensile strength of the specimens with circular and honeycomb pattern is significantly smaller than that of the specimen with strip pattern. The strain at break was highest for 0° orientation and decreases constantly when it is changed to 45° or 90° orientation. The samples with strip, honeycomb, and circular pattern have the lowest strain at break, which correspond to a percent of approximately 2, 4 and 5%, respectively.

The same general trend (qualitative and quantitative) holds for the 3D-printed specimens that undergone thermal annealing (TA) cycles at –40°C. As shown in Fig. 13, for the six patterns, the thermally annealed and untreated 3D-printed specimens were almost identical in their mechanical behavior, with very similar mean Young modulus, tensile strength and tensile strain at break.

For thermally annealed specimens, the Young modulus and tensile strength have relatively consistent results for the three printing orientations. More specifically, the Young modulus of the specimens with 0° orientation (2042.85 ± 46.99 MPa) was slightly higher than that of the specimens with 45° (1991.78 ± 51.29) and 90° (1979.88 ± 56.20 MPa) orientation. This corresponded to a percent difference of maximum 3%. Changing the printing orientation from 0°, to 45° and 90° has no effect on the tensile strength of the thermally annealed 3D-printed samples. The variation between specimens was about 2.5%.

For the cryogenically treated (CT) samples, it is observed that the raster orientation has a significant effect on the Young modulus and tensile strength, as indicated by the stiff slope in Figs. 13a and 13b, respectively. When comparing the raster orientations, Table 6 shows a substantial reduction in Young modulus,

of 10% and 25% for printed material in 45° and 90° orientations, respectively, as compared with 0° orientation. The same general trend holds for tensile strength.

Table 4

Overview of mechanical properties of the untreated 3D-printed samples

Cross-section/ Pattern	Young Modulus [MPa]	Tensile Strength [MPa]	Strain at break	Specific strength [MPa/g]
Full 0°	2068.43 ± 45.53	47.82 ± 1.35	1.2120 ± 0.0002	40.66
Full 45°	2043.97 ± 26.89	46.55 ± 1.49	0.9000 ± 0.238	39.72
Full 90°	2022.53 ± 23.67	46.66 ± 1.13	0.0973 ± 0.018	39.98
Circular	2353.50 ± 18.30	34.30 ± 2.12	0.0176 ± 0.002	45.13
Honeycomb	2368.25 ± 23.65	42.25 ± 1.53	0.0386 ± 0.009	72.59
Strip	2321.60 ± 27.76	51.01 ± 0.71	0.0503 ± 0.009	67.12

Table 5

Overview of mechanical properties of 3D-printed samples after thermal annealing

Cross-section/ Pattern	Young Modulus [MPa]	Tensile Strength [MPa]	Strain at break	Specific strength [MPa/g]
Full 0°	2042.85 ± 46.99	46.35 ± 2.62	1.2380 ± 0.009	39.41
Full 45°	1991.78 ± 51.29	47.34 ± 2.01	0.5790 ± 0.167	40.39
Full 90°	1979.88 ± 56.20	47.20 ± 1.36	0.0780 ± 0.012	40.45
Circular	2258.53 ± 113.77	36.21 ± 1.24	0.0200 ± 0.002	47.64
Honeycomb	2333.58 ± 34.16	41.72 ± 1.11	0.0578 ± 0.008	71.68
Strip	2315.43 ± 23.40	49.83 ± 1.24	0.0494 ± 0.008	65.57

Table 6

Overview of mechanical properties of 3D-printed samples after cryogenic treatment

Cross-section/ Pattern	Young Modulus [MPa]	Tensile Strength [MPa]	Strain at break	Specific strength [MPa/g]
Full 0°	1970.40 ± 43.01	43.74 ± 1.54	0.2645 ± 0.035	37.19
Full 45°	1791.58 ± 10.49	37.94 ± 1.58	0.0422 ± 0.004	32.37
Full 90°	1579.98 ± 32.54	28.86 ± 1.68	0.0247 ± 0.002	24.73
Circular	2017.50 ± 171.26	46.62 ± 1.82	0.0502 ± 0.006	61.34
Honeycomb	1902.83 ± 147.47	35.48 ± 1.14	0.0636 ± 0.018	60.96
Strip	1927.85 ± 51.54	43.16 ± 2.53	0.0696 ± 0.006	56.79

The tensile strength of the 3D-printed specimens decreased from 43.74 ± 1.54 MPa to 28.86 ± 1.68 MPa with increasing printing angle from 0° to 90°. This corresponded to a percent difference of approximately 35%. The tensile strength of cryogenically treated parts was the largest in samples with circular pattern (46.62 ± 1.82 MPa), while the full-cross section specimens with 90° orientation exhibits the smallest value (28.86 ± 1.68 MPa) as shown in Fig. 13b and Table 6.

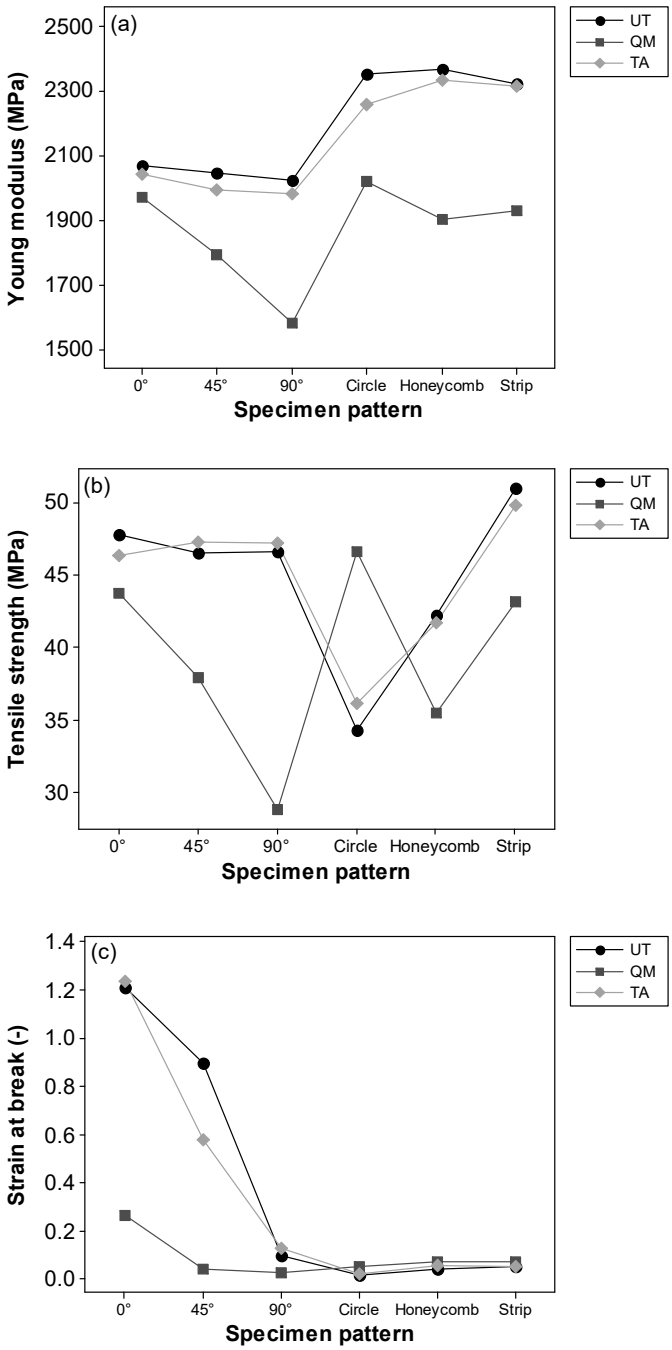

Fig. 13 – Effect of thermal treatment on the mechanical properties of 3D-printed PETG samples (UT – untreated, CT – cryogenic treatment, TA – thermal annealing).

The tensile strain at break of the cryogenically treated samples followed a similar qualitative trend with the untreated samples. The strain at break of the cryogenically treated samples was the largest for the 0° orientation (~26.5%) and decreased asymptotically when the printing orientation changed to 45° (~ 4%) and 90° (~2.5%), as shown in Table 6 and Fig. 13c. The samples with circular, honeycomb and strip patterns, on the other hand, have comparable strains at break (approximately 5 to 7%).

3.3. Statistical analysis

To study the impact of the cryogenic or annealing treatments on the mechanical properties of the 3D-printed PETG specimens, and facilitate the comparison between different sets of experiments, the data were statistically analyzed using the ANOVA and *t*-test at a standard confidence level of $\alpha = 0.05$ [50].

The annealing treatment at –40°C has no statistically significant effect on the Young modulus, tensile strength, and strain at break of the 3D-printed PETG, independently of the printing pattern (all *p*-values greater that any reasonable α).

Statistical analysis of experimental data indicates that the cryogenic treatment has a significant effect on the Young modulus regardless of the printing pattern (since all *p*-value < α, there is evidence for a difference in Young modulus between the cryogenically treated samples and untreated samples).

Furthermore, the cryogenic treatment has a significant influence on the tensile strength at 0.05 significance level (all *p*-value < α), except for the specimens with honeycomb pattern, for which the data do not provide enough evidence to claim that the cryogenic treatment has a significant effect on the tensile strength (the *t*-test statistics is –2.35, with *p*-value of 0.078 greater that α).

Finally, based on statistical analysis it was concluded that the cryogenic treatment has a statistically significant impact on the tensile strain at break of the 3D-printed specimens with 0° (*p*-value = 0.001 < α), 90° (*p*-value = 0.030 < α), and circular (*p*-value = 0.001 < α) pattern. However, there is no statistical evidence for a difference in strain at break between the cryogenically treated and untreated samples with 45° (*t*-stat = –3.60, *p*-value = 0.172), honeycomb (*t*-stat = 1.81, *p*-value = 0.130 > α), and strip (*t*-stat = 2.63, *p*-value = 0.058 > α) pattern.

4. CONCLUSIONS

In this paper, the mechanical properties of 3D-printed PETG after exposure to low, –40°C, and extreme low, –196°C, temperatures were investigated. 3D-printed PETG specimens with different printing patterns were subjected to low and extreme-low temperature by quench method and thermal annealing cycles, respectively. Tension tests were carried out to evaluate the mechanical properties (stiffness,

tensile strength, and elongation at break) of 3D-printed specimens before and after thermal treatments. Based on the experimental results, within the limits of this study, the following conclusions can be drawn:

(i) The selected set of printing parameters produced good quality 3D-printed PETG parts with no visible defects.

(ii) The 3D-printed PETG samples maintain good mechanical properties after thermally annealing cycles at –40°C (100% of mechanical properties of the un-treated samples), indicating that this material can be used to manufacture parts that will be exposed to low temperatures during the operation.

(iii) The mechanical properties of the cryogenically treated samples were generally lower (~10 to 25% depending on the printing angle/pattern) than those of the un-treated and thermally annealed samples. Specimens with 0°, 45° and 90° printing orientation were more sensitive to the cryogenic treatment than those with circular honeycomb and strip patterns.

(iv) The honeycomb, circular and strip patterns allow reaching low weight with a remarkably improved specific strength compared with 0°, 45° and 90° full cross-sections.

(v) From these results, the honeycomb pattern is advised for manufacturing parts that experience low temperature in-service, as it enables an ultra low weight with high mechanical properties.

However, the effect of deep cryogenic treatment on the mechanical properties of the 3D-printed samples need further investigations in order to develop a baseline for the mechanical properties of cryogenically treated samples, that would be very beneficial for design purposes, in the absence of test standards.

Acknowledgements. This research did not receive any specific grant from funding agencies in the public, commercial, or not-for-profit sectors. The authors would like to acknowledge Mr. Gervescu Marius for his assistance with 3D printing.

Received on November 28, 2018

REFERENCES

1. STANSBURY, Jeffrey W., IDACAVAGE, Mike J., *3D printing with polymers: Challenges among expanding options and opportunities*, Dental Mater., **32**, pp. 54–64, 2016.
2. WANG, Xin, JIANG, Man, ZHOU, Zuowan, GOU, Jihua, HUI, David, *3D printing of polymer matrix composites: A review and prospective*, Compos. Part B-Eng., **110**, pp. 442–458, 2017.
3. PARANDOUSH, Pedram, LIN, Dong, *A review on additive manufacturing of polymer-fiber composites*, Compos. Struct., **182**, pp. 36–53, 2017.
4. DIZON, John Ryan, ESPERA Alejandro, CHEN, Qiyi, ADVINCULA, Rigoberto C., *Mechanical characterization of 3D-printed polymers*, Addit. Manuf., **20**, pp. 44–67, 2018.
5. NGO, Tuan D., KASHANI, Alireza, IMBALZANO, Gabriele, NGUYEN, Kate, HUI, David, *Additive manufacturing (3D printing): A review of materials, methods, applications and challenges*, Compos. Part B-Eng., **143**, pp. 172–196, 2018.

6. KIRA, *Wohlers Report 2016 reveals $1 billion growth in 3D printing industry*, http://www.3ders.org/articles/20160405-wohlers-report-2016-reveals-1-billion-growth-in-3d-printing-industry.html, Available online: April 5, 2016, Accessed on: August 28, 2018.
7. Wohlers Report, *3D printing and additive manufacturing state of the industry Annual Worldwide Progress Report*, 2016.
8. DAQUILA, Marianne, GREENE, Tim, CHATURVEDI, Swati, ISHIDA, Eiji, AHUJA, Yash, STOEV, Evelin, GEORGE, Jebin, MEMBRILA, Roberto, LA CROCE, Carla, *IDC's worldwide semiannual 3D printing spending guide, taxonomy, 2018: Update*, July 2018 – Taxonomy – Doc # US44078618.
9. COLUMBUS, Louis, *Roundup of 3D printing market forecasts and estimates* https://www.forbes.com/sites/louiscolumbus/2015/03/31/2015-roundup-of-3d-printing-market-forecasts-and-estimates/#7d2633ae1b30, Available online: March 31, 2015, Accessed on: August 28, 2018.
10. GARTNER, *Gartner survey reveals that high acquisition and start-up costs are delaying investment in 3D printers*, https://www.gartner.com/newsroom/id/2940117, Available online: December 9, 2014, Accessed on: August 28, 2018.
11. FORBES, *The future of 3-D printing***,** https://www.forbes.com, January 2018, Available Online: January 23, 2018, Accessed on: August 28, 2018.
12. RAYNA, Thierry, STRIUKOVA, Ludmila, *From rapid prototyping to home fabrication: How 3D printing is changing business model innovation*, Technol. Forecast. Soc., **102**, pp. 214–224, 2016.
13. AHN, Sung-Hoon, MONTERO, Michael, ODELL, Dan, ROUNDY, Shad, WRIGHT, Paul, *Anisotropic material properties of fused deposition modeling ABS*, Rapid Prototyping J., **8**, pp. 248–257, 2002.
14. LEE, Sunyong, KIM, Sunggeun, KIM, Hyounjin, AHN, Sung-Hoon, *Measurement of anisotropic compressive strength of rapid prototyping parts*, J. Mater. Process. Technol., **187–188**, pp. 627–630, 2007.
15. ZIEMIAN, Constance, SHARMA, Mala, ZIEMIAN, Sophia, *Anisotropic mechanical properties of ABS parts fabricated by fused deposition modelling* (Chap. 7), in: *Mechanical Engineering* (ed. M. Gokcek), pp. 159–180, IntechOpen, 2012.
16. GUESSASMA, Sofiane, BELHABIB, Sofiane, NOURI, Hedi, HASSANA, Omar Ben, *Anisotropic damage inferred to 3D printed polymers using fused deposition modelling and subject to severe compression*, Eur. Polym. J., **85**, pp. 324–340, 2016.
17. LETCHER, Todd, RANKOUHI, Behzad, JAVADPOUR, Sina, *Experimental study of mechanical properties of additively manufactured ABS plastic as a function of layer parameters*, ASME 2015 International Mechanical Engineering Congress and Exposition, Paper No. IMECE2015-52634, pp. V02AT02A018, 2015.
18. LEE, B.H., ABDULLAH, Jafri Malin, KHAN, Zahid Akhtar, *Optimization of rapid prototyping parameters for production of flexible ABS object*, J. Mater. Process. Technol., **169**, pp. 54–61, 2005.
19. SOOD, Anoop Kumar, OHDAR, Raj, MAHAPATRA, Siba Sankar, *Experimental investigation and empirical modelling of FDM process for compressive strength improvement*, J. Adv. Res., **3**, pp. 81–90, 2012.
20. DAWOUD, Michael, TAHA, Iman, EBEID, Samy, *Mechanical behaviour of ABS: An experimental study using FDM and injection moulding techniques*, J. Manuf. Process., **21**, pp. 39–45, 2016.
21. TIAN, Xiaoyong, LIU, Tengfei, YANG, Chuncheng, WANG, Qingrui, LI, Dichen, *Interface and performance of 3D printed continuous carbon fiber reinforced PLA composites*, Compos. Part A-Appl. S., **88**, pp. 198–205, 2016.
22. CHACÓN, Jesus, CAMINERO, Miguel Angel, GARCÍA-PLAZA, Eustaquio, NÚÑEZ, Pedro J., *Additive manufacturing of PLA structures using fused deposition modelling: Effect of process parameters on mechanical properties and their optimal selection*, Mater. Design, **124**, pp. 143–157, 2017.

23. GOMEZ-GRAS, Giovanni, JEREZ-MESA, Ramon, TRAVIESO-RODRIGUEZ, J. Antonio, LLUMA-FUENTES, Jordi, *Fatigue performance of fused filament fabrication PLA specimens*, Mater. Design, **140**, pp. 278–285, 2018.
24. KARALEKAS, Dimitris, AGGELOPOULOS, A., *Study of shrinkage strains in a stereolithography cured acrylic photopolymer resin*, J. Mater. Process. Technol., **136**, pp. 146–150, 2003.
25. KANTAROS, Antreas, KARALEKAS, Dimitris, *Fiber Bragg grating based investigation of residual strains in ABS parts fabricated by fused deposition modeling process*, Mater. Design, **50**, pp. 44–50, 2003.
26. CASAVOLA, Caterina, CAZZATO, Alberto, MORAMARCO, Vincenzo, PAPPALETTERA, Giovanni, *Residual stress measurement in fused deposition modelling parts*, Polym. Test., **58**, pp. 249–255, 2017.
27. ZHANG, Wei, WU, Amanda S., SUN, Jessica, QUAN, Zhenzhen, GU, Bohong, SUN, Baozhong, COTTON, Chase, HEIDER, Dirk, CHOU, Tsu-Wei, *Characterization of residual stress and deformation in additively manufactured ABS polymer and composite specimens*, Compos. Sci. Technol., **150**, pp. 102–110, 2017.
28. FARBMAN, Daniel, MCCOY, Chris, *Materials testing of 3D printed ABS and PLA samples to guide mechanical design*, ASME 2016 11th International Manufacturing Science and Engineering Conference, June 2016, DOI: 10.1115/MSEC2016-8668.
29. WU, Wenzheng, GENG, Peng, LI, Guiwei, ZHAO, Di, ZHANG, Haibo, ZHAO, Ji, *Influence of layer thickness and raster angle on the mechanical properties of 3D-printed PEEK and a comparative mechanical study between PEEK and ABS*, Materials, **8**, pp. 5834–5846, 2015.
30. LANZOTTI, Antonio, GRASSO, Marzio, STAIANO, Gabriele, MARTORELLI, Massimo, *The impact of process parameters on mechanical properties of parts fabricated in PLA with an open-source 3-D printer*, Rapid Prototyping J., **21**, *5*, pp. 604–617, 2015.
31. BROWN, Peter, *Video: Watch the winning mouser ISS design project in action* https://electronics360.globalspec.com/article/8611/video-watch-the-winning-mouser-iss-design-project-in-action, Available Online: May 4, 2017, Accessed on: August 28, 2018.
32. NASA Science Beta, *Staying cool on the ISS*, https://science.nasa.gov/science-news/science-at-nasa/2001/ast21mar_1, Available Online: March 20, 2001, Accessed on: August 28, 2018.
33. HECHTEL, Keith, *Design considerations for the use of plastic materials in cryogenic environments*, Curbell Plastics Inc., October, 2014, https://www.curbellplastics.com, Accessed on: August 28, 2018.
34. LETCHER, Todd, WAYTASHEK, Megan, *Material property testing of 3D-printed specimen in PLA on an entry-level 3D printer*, Proceedings of the ASME 2014 International Mechanical Engineering Congress & Exposition (IMECE2014), Montreal, 2014, DOI:10.1115/IMECE2014-39379.
35. DURGUN, Ismail, ERTAN, Rukiye, *Experimental investigation of FDM process for improvement of mechanical properties and production cost*, Rapid Prototyping J., **20**, pp. 228–235, 2014.
36. QUAN, Zhenzhen, LARIMORE, Zachary, WU, Amanda, YU, Jianyong, QIN, Xiaohong, MIROTZNIK, Mark, SUHR, Jonghwan, BYUN, Joon-Hyung, OH, Youngseok, CHOU, Tsu-Wei, *Microstructural design and additive manufacturing and characterization of 3D orthogonal short carbon fiber/acrylonitrile-butadiene-styrene preform and composite*, Compos. Sci. Technol., **126**, pp. 139–148, 2016.
37. SONG, Yichi, LI, Yizhuo, SONG, Wenzhe, YEE, Ka-Lai, LEE, Koon-Yang, TAGARIELLI, Vito, *Measurements of the mechanical response of unidirectional 3D-printed PLA*, Mater. Design, **123**, pp. 154–164, 2017.
38. WEISS, Klaus-Peter., BAGRETS, Nadezda, LANGE, Christian, GOLDACKER, Wilfried, WOHLGEMUTH, Jonas, *Thermal and mechanical properties of selected 3D printed thermoplastics in the cryogenic temperature regime*, IOP Conf. Series: Materials Science and Engineering, 2015.

39. CRUZ, P., SHOEMAKE, Elijah, ADAM, Patrick, LEACHMAN, Jacob, *Tensile strengths of polyamide based 3D printed polymers in liquid nitrogen*, IOP Conf. Series: Materials Science and Engineering, 2015.
40. BARTOLOMÉ, Elena, BOZZO, Bernat, SEVILLA, P., MARTÍNEZ-PASARELL, Olga, PUIG, Teresa, GRANADOS, Xavier, *ABS 3D printed solutions for cryogenic applications*, Cryogenics, **82**, pp. 30–37, 2017.
41. TYMRAK, Brennan, KREIGER, Megan, PEARCE, Joshua, *Mechanical properties of components fabricated with open-source 3-D printers under realistic environmental conditions*, Mater. Design, **58**, pp. 242–246, 2014.
42. https://www.3dxtech.com.
43. ISO 527:2012 Plastics – Determination of tensile properties.
44. Cura 15.02.1 software.
45. GALETA, Tomislav, RAOS, Pero, STOJŠIĆ, Josip, PAKŠI, Ivana, *Influence of structure on mechanical properties of 3D printed objects*, Procedia Eng., **149**, pp. 100–104, 2016.
46. STAN, Felicia, STANCIU, Nicoleta-Violeta, FETECAU, Catalin, *Melt rheological properties of ethylene-vinyl acetate/ Multi-walled carbon nanotube composites*, Compos. Part B-Eng., **110**, pp. 20–31, 2017.
47. ISLAM, Nazrul, BOSWELL, Brian, PRAMANIK, Alokesh, *Dimensional accuracy achievable by three-dimensional printing*, Chap. 28, in: "IAENG Transactions on Engineering Sciences", (eds. S.-I. Ao, A.H.-S. Chan, H. Katagiri, L. Xu), Taylor & Francis Group, 2014, pp. 263–268.
48. SCHMUTZLER, Christoph, ZIMMERMANN, Alexander, ZAEH, Michael F., *Compensating warpage of 3D printed parts using free-form deformation*, Procedia CIRP, **41**, pp. 1017–1022, 2016.
49. TORRADO PEREZ, Angel R., ROBERSON, David A., WICKER, Ryan B., *Fracture surface analysis of 3D-printed tensile specimens of novel ABS-based materials*, J. Fail. Anal. Prev., **14**, pp. 343–353, 2014.
50. MONTGOMERY, D.C., *Design and analysis of experiments*, 8th Edition, Wiley, Danvers, Massachusetts, USA, 2012.